Cite this: *CrystEngComm*, 2011, **13**, 4866

www.rsc.org/crystengcomm

PAPER

Crystalline perfection, EPR, prism coupler and UV-VIS-NIR studies on Cz-grown Fe-doped $LiNbO_3$: A photorefractive nonlinear optical crystal

Satya Kumar Kushwaha, Kamlesh Kumar Maurya, Narayanasamy Vijayan and Godavarthi Bhagavannarayana*

Received 25th November 2010, Accepted 6th May 2011
DOI: 10.1039/c0ce00892c

The Fe-doped (0.05 mol%) lithium niobate ($LiNbO_3$) bulk single crystal was gown by the Czochralski (Cz) method using a co-axial two zone low thermal gradient furnace. The crystalline perfection of the grown crystal was evaluated by high resolution X-ray diffractometry which showed that it does not contain any structural grain boundaries, and the dopants predominantly occupied vacancy sites of Li^+ in the lattice. Electron paramagnetic resonance studies revealed the incorporation of Fe^{3+} ions at Li sites. The Z-cut optically polished 450 μm thick wafer was used for birefringence measurements on a prism coupler spectrometer with 632.8 nm wavelength and it was found that the difference in refractive index (Δn) for ordinary and extraordinary rays is 0.0833. The optical transmission/absorption spectra were studied by UV-VIS-NIR spectroscopy and this showed that the grown crystal has good optical sensitivity for 482 nm wavelength radiation. The present studies reveal that the crystal grown with a two zone low thermal gradient furnace has very good device properties which are needed for holographic data storage applications.

Introduction

Lithium niobate (LN), a nonlinear optical (NLO) material in its single crystal form has been well proved as a potential and unique material for its use in advanced photonic device applications like second-harmonic generation (SHG), optical switching, optical modulators, holographic data storage, acousto-optic and ferroelectric.[1–5] The transition and rare earth metal ions (Fe, Mn, Cu and Ce) improve the data storage capabilities of LN by improving its photorefraction efficiency.[1,6–8] Fe-doped LN (Fe : LN) was also found to be suitable for the pyroelectric infrared sensors and X-ray generation applications.[9] The dopants incorporate homogeneously throughout the crystal lattice only up to a certain level of doping concentration according to the accommodation capability of the lattice and the size and ionic state of the dopants.[10,11] However, when the concentration of dopants in the crystal increases, the high geometric strains develop in the lattice and while the crystal tries to relax, dynamics of point defects take place and result in agglomeration of point defects, formation of dislocations[12] and finally leads to structural boundaries.[13] These defects mask or partially/completely deteriorate some of the anisotropic physical properties of single crystals and reduce the efficiency of the devices made out of these crystals.[11,14–17] Therefore, to exploit the full efficiency of the doped crystals for the particular desired application, these must be at least free from the dislocations and grain boundaries,[16,18,19] and hence great care is needed to grow good quality single crystals. Due to continuous miniaturization of the modern devices based on single crystals, assessment of the crystalline perfection becomes more and more important in the modern advanced technology. Different direct and indirect techniques such as Raman spectroscopy, FT–IR, X-ray topography, EPR, NMR, optical homogeneity, transmission electron microscopy[20–25] techniques have been employed to analyze the structural defects in lithium niobate single crystals. HRXRD has also been found to be one of the most suitable methods to assess the crystalline perfection and to reveal the presence of commonly observed structural grain boundaries in bulk crystal domain.[18,26] Successful removal of such defects by thermal annealing at low raising/cooling rates and the effect of such treatments on crystalline perfection which influences the device properties have been demonstrated with the help of HRXRD.[18] The transition metals lead to a change in the refractive index and optical transparency[27–29] of $LiNbO_3$. It is well known that during a cooling cycle LN single crystals undergo a phase transition at 1140 °C and it slightly varies with doping using different dopants.[30] Due to this transition, the structure changes followed by volume changes[31] leading to cracks and structural boundaries as mentioned above.[18] Though such a large number of studies have been reported, some more precise and in-depth studies are still necessary on the strategic material of title material (LN). In continuation of such investigations, we report here (i) the growth of good quality bulk Fe : LN single crystals by the indigenously developed Czochralski (Cz) crystal puller,[32] (ii) evaluation of crystalline perfection by high-resolution X-ray diffractometry (HRXRD) to reveal more information about the effect of

National Physical Laboratory, Council of Scientific and Industrial Research, New Delhi, 110012, India. E-mail: bhagavan@mail.nplindia.ernet.in

Fe-doping and the associated antisitic defects, (iii) electron paramagnetic resonance (EPR) spectrometry analysis to study the incorporated iron and identify their paramagnetic sites, (iv) the prism coupler experiments to estimate the difference in the refractive index Δn accurately in ordinary and extraordinary rays and (v) optical transmittance and absorbance study in the UV-VIS-NIR wavelength range. The photorefractive properties of $LiNbO_3$ single crystals are enhanced by doping with iron and, as reported,[8] at ~0.06 wt% of Fe_2O_3 doping $LiNbO_3$ exhibited the best performance for multiplexing capability related to holographic applications. Due to this reported doping level of proven advantage, the authors have grown the bulk crystal of $LiNbO_3$ with 0.05 mol% Fe_2O_3 concentration, which is close to that reported.

Experimental

Crystal growth

The single crystal of Fe : LN (0.05 mol % Fe_2O_3) has been successfully grown by a Cz crystal puller developed in-house . To ensure the smooth and uniform pulling two stainless steel rods, one with a square cross-section having surface planarity of 5 μm over its entire one meter length and another with a circular cross-section have been used, which act as guides to the entire pulling mechanism along with the platform on which the seed assembly rests.[33] The platinum crucible of 50 mm diameter and 40 mm height was used to grow the crystal at ~1523 K in a two zone furnace. The schematic of the furnace is shown in Fig. 1(a). The lower zone is the 30 kW radio-frequency (30 kHz) heating (RFH) coil which is the main source of heat to the platinum crucible to melt the charge and to provide continuous heating while the crystal is growing. To lower the temperature gradient above the RFH and also for a well controlled post growth cooling, a co-axial resistive post growth heater (RPGH) is placed just above the RFH. Before starting the growth and also before switching on the RFH, RPGH has been kept at a constant temperature around 1073 K by giving a fixed voltage through a precise variac. Then the RFH switches on and the required temperature is obtained through a programmable Eurotherm controller (2404) with ± 0.01 K stability. When the RFH switches on, the temperature in the resistive zone increases. Fig. 1(b) shows the vertical temperature profile of the furnace, recorded starting from the bottom of the empty crucible. As seen in the Fig. 1(b), due to the presence of resistive heating, a good profile needed to grow lengthy crystals of the order of 100 to 125 mm has been obtained. During the growth process, a temperature gradient of ~14 K cm^{-1} was maintained just above the melt level by RPGH to avoid the formation of extended structural defects like twins and grain boundaries which often occur at the early stage of crystallization from seed.[34]

The starting 4 N purity (Sigma Aldrich) materials of $LiNbO_3$ and 0.05 mol% of Fe_2O_3 were properly mixed and sintered at 1000 °C for 8 h before melting. The melted charge was left for 4 h for homogeneous mixing of dopants. A good quality 20 mm long with square cross section (5 × 5 mm^2) crystal cut along [001] was used as a seed to grow the bulk crystal. After nucleation of a crystal at the seed, the temperature of the lower RFH zone was gradually reduced to increase the diameter of the growing crystal.

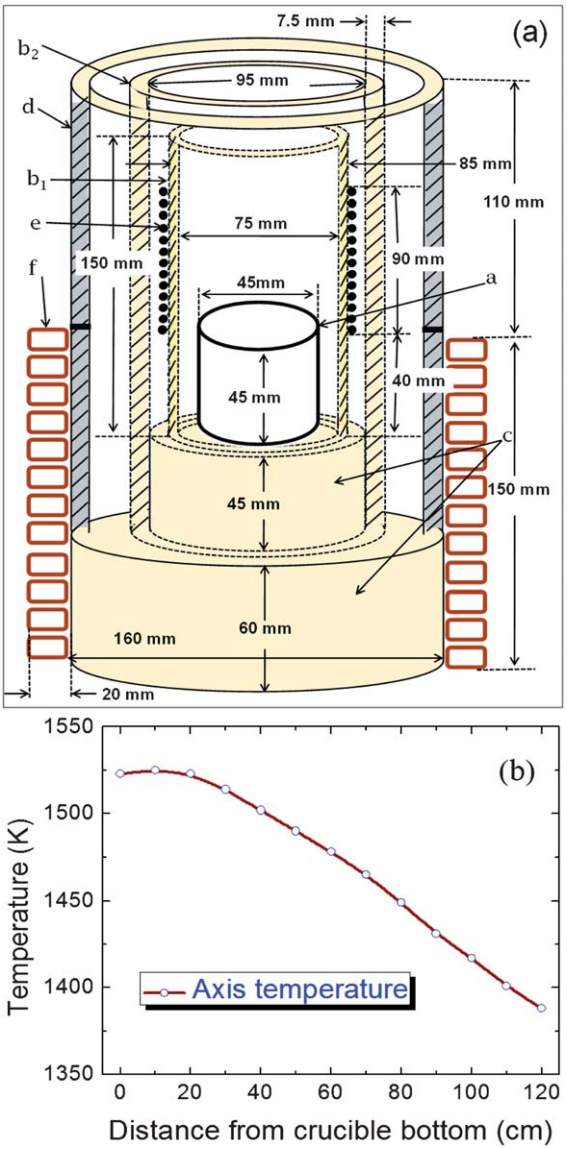

Fig. 1 (a) The schematic of furnace in which a, b_1, b_2, c, d, e and f represent respectively platinum crucible, inner alumina muffle, outer alumina muffle, ceramic blocks, asbestos sheet, resistive heater and radio frequency coil. Curve (b) shows the axial temperature profile.

The pulling rate of crystal was precisely maintained at 2 mm h^{-1} with constant rotation of 35 rpm over the complete growth process. After the growth at 1528 K, the crystal was cooled at a very slow rate of 12 K h^{-1} up to 1273 K to avoid crack formation during the phase transition[35] at ~1423 K. Later, the cooling rate was increased to 20 K h^{-1} until the temperature reached 1073 K and then further increased to 40 K h^{-1} until the temperature reached ~600 K by controlling both RFH and RPGH heating. Then RFH was switched off and by controlling RPGH alone, the temperature was reduced to room temperature with the previous cooling rate of 40 K h^{-1}. Such growth conditions facilitated us to obtain a 50 mm long and ~20 mm diameter bulk single crystal of Fe : LN without any visible voids or cracks. The harvested crystal is shown in Fig. 2. It is visibly quite transparent, but due to Fe doping, it adopted a slightly brown

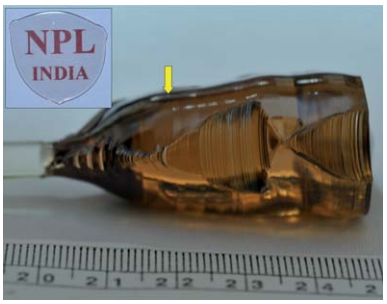

Fig. 2 Fe-doped $LiNbO_3$ single crystal grown along [001]. Inset shows a Z-cut and optically polished wafer from the region of boule indicated by the arrow.

color. An optically polished Z-cut crystal wafer with ~450 μm thickness is shown in the inset of Fig. 2. The arrow in the figure indicates the region of the crystal boule from where the wafer was cut.

High resolution multicrystal X-ray diffractometry

The as grown Fe : LN was characterized by employing the multicrystal X-ray diffractometer (MCD) developed in-house,[36] by recording the high resolution X-ray diffraction/rocking curve (RC) in order to assess its crystalline perfection. A schematic of the MCD is shown Fig. 3. In this system, a fine focus (0.4 × 8 mm^2; 2 kW Mo) X-ray source energized by a well-stabilized Philips X-ray generator (PW 1743) was employed. The well-collimated and monochromatic $MoK_{\alpha 1}$ beam obtained from the three monochromator Si crystals set in dispersive (+,−,−) configuration has been used as the exploring X-ray beam. The details about the importance of dispersive configuration and the experimental procedure are described in the earlier publications.[17,37] This arrangement improves the spectral purity ($\Delta\lambda/\lambda \ll 10^{-5}$) of the $MoK_{\alpha 1}$ beam. The divergence of the exploring beam in the horizontal plane (plane of diffraction) was estimated to be ≪3 arcsec. Due to the dispersive configuration, though the lattice constant of the monochromator crystal(s) and the specimen are different, the unwanted experimental dispersion broadening in the diffraction curve of the specimen crystal is insignificant. The specimen can be rotated about a vertical axis, which is perpendicular to the plane of diffraction, with a minimum angular interval of 0.4 arcsec. The RC was recorded for (006) diffraction planes by changing the glancing angle (angle between the incident X-ray beam and the surface of the specimen) around the Bragg diffraction peak position θ_B (taken zero as reference point) starting from a suitable arbitrary glancing angle (θ). The detector was kept at the same angular position $2\theta_B$ with wide opening for its slit, the so-called ω-scan. The importance of the ω-scan chosen in the present experiments and its advantage over $2\theta - \theta$ or $2\theta - \omega$ scan is as follows. As mentioned above, in LN crystals, structural grain boundaries are expected.[13] In the case of a $2\theta - \theta$ scan, the experimentally obtained RC contains the information about a single grain which we align for the scan and the rocking curve is expected to be very sharp as the detector with a narrow slit will not receive diffracted intensities from the other grains which are misoriented to the grain under investigation (*i.e.* aligned for diffraction) or the diffuse scattering from point defects and their aggregates. Whereas in the relatively simple omega scan, with a sufficiently wide slit for the detector, if the crystal contains structural grain boundaries, we get all the peaks in the RC. On the other hand in the omega scan if we get a single peak, it confirms that the specimen crystal has a single domain with a single orientation. It is worth mentioning here that unless the exploring beam is very fine (like $\Delta\lambda/\lambda \sim 10^{-5}$ and horizontal divergence ≪3 arcsec), the RC in an omega scan do not yield resolved peaks except a very broad peak though the crystal contains grain boundaries. Using this in-house developed diffractometer, we have found the splitting of rocking curves recorded in the omega scan in a variety of crystals like LN,[13] LiF,[33] BGO,[38] oxalic acid doped ADP,[19] L-threonine doped KDP,[39] urea doped ZTS[17] and have demonstrated that these are due to very low and low angle structural grains with the help of section topographs. With the help of powder XRD, it was also confirmed that this type of minute splitting in the RC is not due to different phases even in the doped crystals.[17,19] As described in our recent article,[40] the theoretical FWHM is nearly proportional to the wavelength of the exploring X-ray beam and hence to get more reliable information from a rocking curve, $MoK_{\alpha 1}$(λ = 0.70926 Å) is better than that of $CuK_{\alpha 1}$ (λ = 1.54056 Å). In view of these advantages, an omega scan in HRXRD with this specially designed diffractometer was adopted.

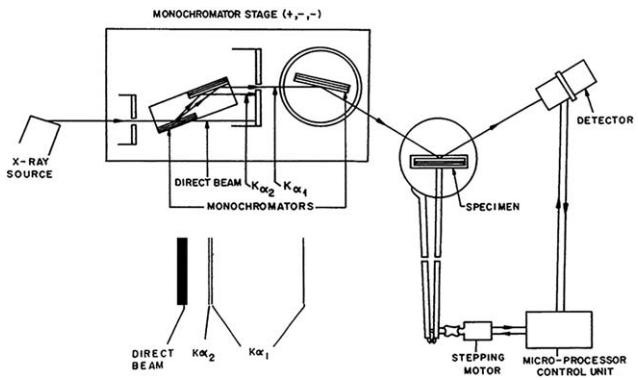

Fig. 3 Schematic of the multicrystal X-ray diffractometer developed at NPL. Inset shows the MoK_α doublet and the isolated K_{α_1} beam.

EPR spectroscopy

EPR study of grown (Fe : LN) single crystal was carried out by employing a Brukar Biospin A300 X-band EPR spectrometer. The measurements were carried out at a radio frequency of 9.462 GHz with the modulation frequency of 100 kHz at T = 297 K. A Z-cut rectangular crystal (1 × 3 × 5 mm^3) was placed in the cavity keeping the c-axis parallel to the applied magnetic field. EPR parameters of the crystal like peak-to-peak line width (ΔH_{pp}), g-value and uncompensated spin concentrations (N_S) were calculated.

Prism coupler spectrometer

The refractive indices for ordinary and extraordinary wave propagation for the Fe : LN crystal was measured by Metricon prism coupler spectrometer (Model 2010/M) at room temperature with an accuracy of ±0.0005 and resolution of ±0.0003 for

the refractive index. The standard rutile prism with a refractive index of 2.8659 was used to couple the 632.8 nm He–Ne laser beam to the crystal wafer, and a pixel array detector was set to collect the emergent beam. The schematic geometry for a prism in contact with a wafer and laser beam is shown in Fig. 6(a). The Z-cut specimen wafer of thickness 450 μm with a surface roughness of $\sim\lambda/10$ was used. The wafer was coupled with the prism by the coupling head. The whole assembly consisting of a prism, a crystal wafer, an array detector and a coupling head was made to rotate with respect to incident laser beam with the rotation step of 1.5 min. The reflected intensity *vs.* step variation patterns were recorded to locate the knee position for ordinary and extraordinary polarized laser beams.

UV-Vis-NIR optical spectroscopy

The optical transparency and absorption spectra for the prepared wafer over the entire UV-VIS-NIR wavelength spectrum (200–1100 nm) was recorded on a Perkin Elmer Lambda 35 spectrophotometer with the incident beam normal to the surface (Z-cut) at the step size of 1 nm.

Results and discussion

High-resolution XRD analysis

Fig. 4(a) shows the HRXRD rocking curve for (006) diffraction planes of the Fe : LN crystal recorded in a symmetrical Bragg geometry. The single peak shows that the crystal does not contain any structural grain boundaries and cracks though LN is prone to get boundaries and cracks as it undergoes structural phase transitions associated with volume changes during the cooling cycle. The full width at half maximum of the diffraction curve is 80 arcsec which is quite high in comparison with that of the theoretical RC[41] (2.6 arcsec) [Fig. 4(b)] or with that of undoped specimen[13] (Bhagavannarayana, G. (2005)) and indicates that the crystal is not free from microscopic defects, *i.e.* point defects and their aggregates.[36,42,43] To understand these defects, first it is worth observing the asymmetry of the curve. For a particular angular deviation ($\Delta\theta$) of glancing angle with respect to the peak position, the scattered intensity is much more in the negative direction in comparison to that of the positive direction. This feature clearly indicates that the crystal contains predominantly vacancy type defects rather than interstitial defects. This can be well understood by the fact that due to vacancy defects, as shown schematically in the inset, the lattice around these defects undergoes tensile stress and the lattice parameter d (interplanar spacing) increases and leads to more scattered (also known as diffuse X-ray scattering) intensity at slightly lower glancing angles with respect to the exact Bragg angle (θ_B) as d and $\sin\theta_B$ are inversely proportional to each other in the Bragg equation ($2d\sin\theta_B = n\lambda$; n and λ being the order of reflection and wavelength respectively, which are fixed).[19] It may be mentioned here that the variation in lattice parameter is confined very close to the defect core which gives the scattered intensity only close to the Bragg peak. Long range order could not be expected and hence change in the lattice parameter is not expected either.[33] It may be worth mentioning here that the Fe-dopants are more or less statistically distributed in the crystal. If the dopants or impurities are not statistically distributed, but

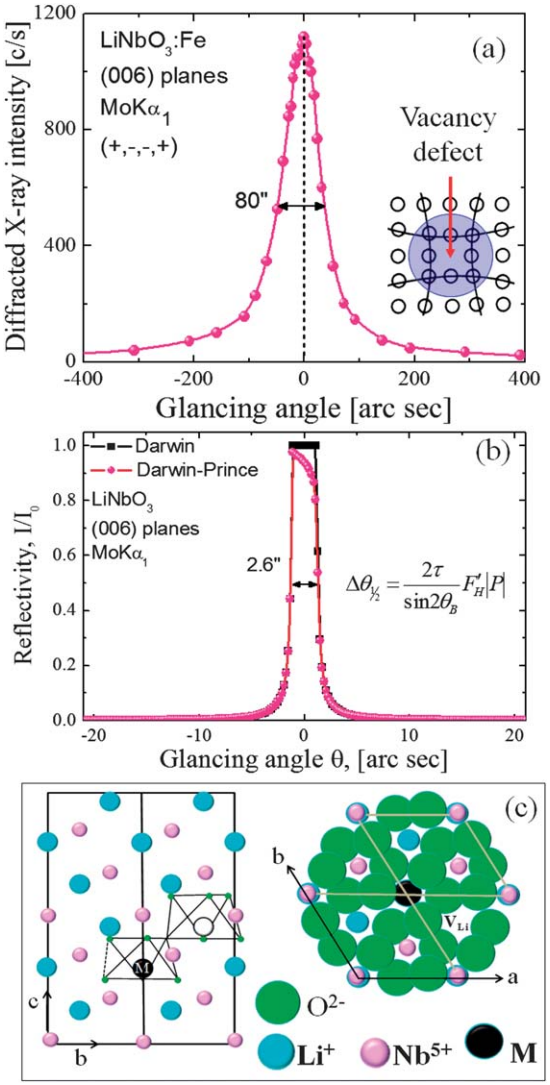

Fig. 4 (a) The recorded rocking curve for (006) diffraction planes of Z-cut specimen, (b) the theoretical rocking curve obtained for LN and (c) schematic of hexagonal unit cell (courtesy of ref. 15) of doped crystal and bonding nature around Li vacancy, arrangement of constituent atoms projected on (0001) plane. M denotes iron at Li^+ site and V_{Li} represents a Li vacancy.

distributed here and there as macroscopic clusters, then the strain generated by such clusters is larger leading to cracks and structural grain boundaries which can be seen very clearly in HRXRD curves with additional peak(s) as observed in our recent study on urea-doped crystals in ZTS at various levels of doping.[17] However, in the present experiments the RC of Fe : LN does not contain any additional peak and indicates the absence of clustering of Fe at macroscopic level.

The above analysis clearly indicates that the Fe : LN contains vacancy defects. In the Fe : LN crystal, Fe could exist in two states Fe^{2+} and Fe^{3+}. The smaller Fe^{3+} and Fe^{2+} ions (64.5 and 78 pm, ionic radii) respectively replace three and two larger Li^+ ions (76 pm; ionic radius) leaving two and one vacancies respectively in the crystal lattice due to charge compensation.[11] The crystal lattice with incorporated metal ion (M) and Li^+ vacancy (V_{Li}) is

shown in Fig. 4(c) through the schematic of hexagonal unit cell and projected view of (0001) plane of crystal lattice.[15] The asymmetry of rocking curve also confirms the congruent nature of the grown crystal, otherwise for stoichiometric phase, the iron ions would have replaced the Nb^{5+} ions of smaller ionic radius (76 pm) and give higher scattered intensity in the +ve direction with respect to the peak position. This is well understood from the converse explanation given to the vacancies in the above paragraph. The larger iron ions which occupy the vacancies in place of smaller Nb^{5+} ions could compress the lattice around them, leading to a decrease in the *d* parameter which results in more scattering at larger angles. It may be mentioned here that in our earlier investigations[13] we had grown Fe-doped LN single crystals which were having the structural grain boundaries in the as-grown state. However, in the present investigation due to incorporation of resistive furnace (RPGH), which results a low thermal gradient, we could grow bulk crystals free from structural defects like voids, cracks and structural grain boundaries.

EPR analysis

The dopants in lithium niobate crystals produce the photochromic centers and are able to change the photorefractive properties.[6,44,45] Electron spin resonance was found to be a suitable method to characterize these photochromic centers.[46] The recorded EPR spectrum of the grown Fe : LN crystal is shown in Fig. 5. The originated spectrum with clear peaks is due to the presence of dopants in Fe^{3+} form at the Li sites of LN. All the resonance peaks corresponding to their respective transitions are quite clear, which supports the homogeneous distribution of dopants in the entire crystal lattice in tune with HRXRD results. A small sharp resonance line at ~3400 G with a magnified view in the inset corresponds to Li with $g = 2.0023$. The observed spectrum of Fe^{3+} depicts that the doped ions are in axial symmetry at the substitutional sites of Li^{+} with the symmetry axis parallel to the crystallographic *c*-axis.[47]

Birefringence analysis

Lithium niobate is an excellent photorefractive crystal and its refractive index varies greatly in the presence of transition metals, even in trace amounts.[27] Therefore, it is important to measure the refractive index of the grown crystals very accurately; the prism coupler was found to be an ideal method to calculate the ordinary and extraordinary refractive indices with high accuracy.[48–50] The optically polished wafer surface was placed in good contact with the base of a right angled rutile prism and the laser beam (632.8 nm) was coupled into the crystal wafer. When the laser beam in the prism matches the propagation constant of modes in the wafer, the beam is coupled into the wafer. The transverse electric (TE) and transverse magnetic (TM) guided-mode spectra are shown in Fig. 6(b) and 6(c) respectively. The sharp fall in the intensity in the spectra indicates the good coupling of the crystal wafer with the prism and there is no scattering of beam at the coupling interface. The located knee positions in the spectra were used to calculate the refractive indices. The calculated ordinary and extraordinary refractive indices n_{TE} and n_{TM} are found to be 2.2880 and 2.2047 respectively with the difference ($\Delta n = n_{TE} - n_{TM}$) of 0.0833. Both of the calculated indices for our crystal wafer are slightly higher than

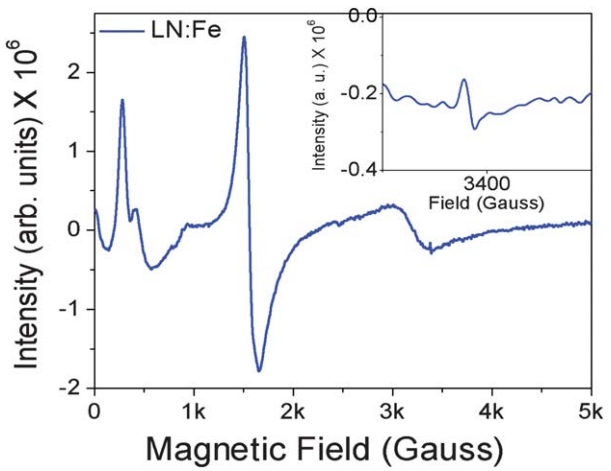

Fig. 5 EPR spectrum recorded at room temperature; inset shows the close view of the signal at ~3380 Gauss owing to the Li metal.

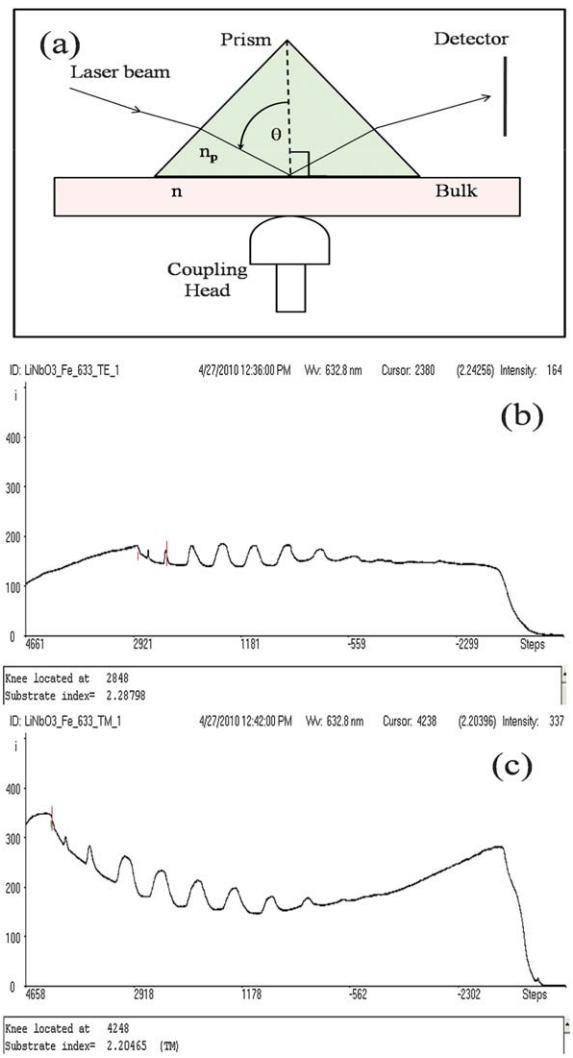

Fig. 6 (a) Schematic of prism coupler spectrometer (b) and (c) are respectively the reflection patterns recorded for TE and TM modes for the Z-cut wafer shown in Fig. 2.

that of earlier reported for pure LN.[29,51,52] The evaluated indices and recorded reflection spectra indicate that the grown crystal is of good optical quality and free from the macroscopic structural defects like voids, dislocations and grain boundaries as revealed by HRXRD. However the slight increment in n_{TE} and n_{TM} may be attributed to the doping of iron. The incorporated iron in Fe : LN exists in Fe^{2+} and Fe^{3+} two valance states which cause the redistribution of electronic charge in the crystal and create the space charge fields. The space charge field interacts with the incident electromagnetic radiation and change the refractive indices n_o and n_e through electro-optic effect.[6] The electrons are excited from Fe^{2+} ions and redistributed due to the drift in electric field or photovoltaic effect and are finally trapped as Fe^{3+} ions, which gives rise to build up space charge field.[27,51] In earlier studies on Mg doped lithium niobate, the change in refractive indices (Δn) for 532 nm wavelength found to be decreased, whereas for 1064 nm its value increased.[53]

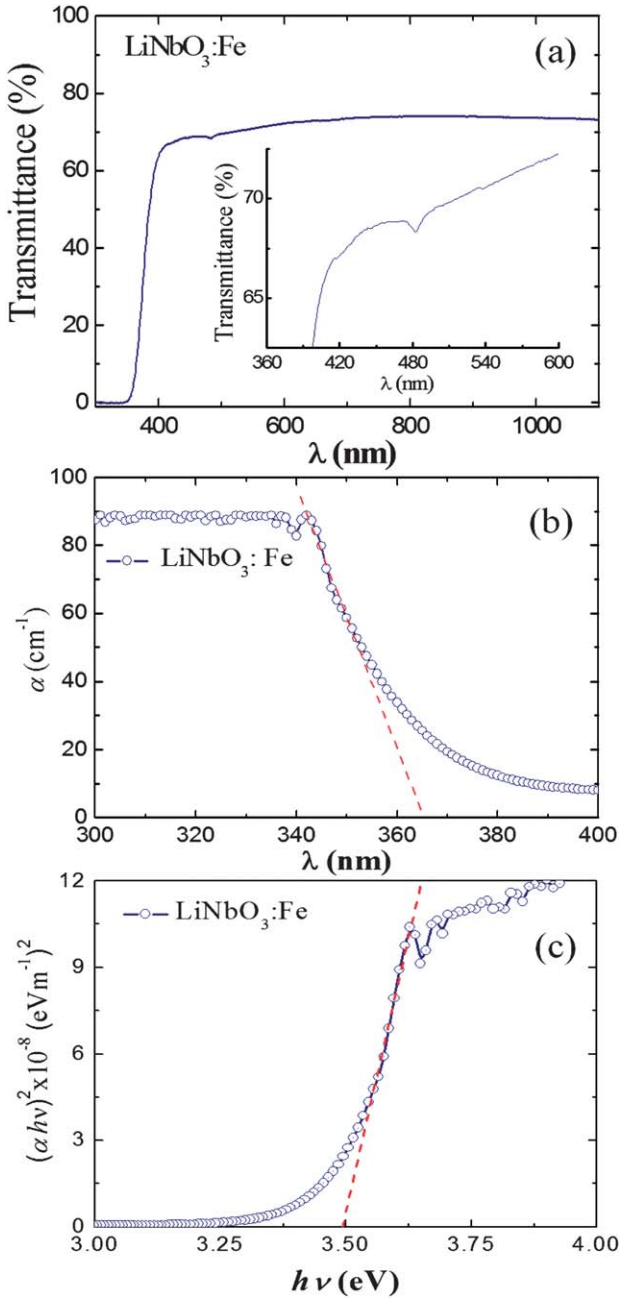

Fig. 7 (a) The optical transparency spectrum of Fe doped LN wafer; the inset shows the sharp absorption, (b) absorption co-efficient spectrum in UV region and (c) $(\alpha h\upsilon)^2$ *vs.* $h\upsilon$ spectrum indicates the energy band gap of crystal.

UV-VIS analysis

The recorded transmittance spectrum for the wafer is shown in Fig. 7(a). The spectrum indicates that the grown crystal is highly transparent for the wavelength range from 375 to 1100 nm, whereas below 375 nm, it is highly absorbing. The high transparency indicates that most of the Fe is statistically distributed in the entire crystal without forming macroscopic clusters. The magnified view of the spectrum in 360–600 nm range in the inset of Fig. 7(a) visualizes the sharp absorption for 482 nm. The 482 nm photons excite the electrons of Fe^{2+} to the conduction band and are trapped by Fe^{3+} ions. This absorption is attributed to the presence of iron in the form of Fe^{2+} ions (antisitic defects)[46] and the spin forbidden d–d transition of Fe^{3+} ions. However, from the spectrum it is clear that there is no clear broad band except a slight lowering of transparency, which has been otherwise reported due to the transfer transitions[54] of Fe^{2+}–Nb^{5+}. The sharpness of the valley indicates the existence of iron in the crystal lattice in Fe^{3+} form.[55] The absorption coefficient in Fig. 7 (b) indicates the increase in the optical absorption and shifting of the absorption edge towards higher wavelengths for grown Fe : LN crystal as compared to that of reported pure LN.[56] Fig. 7(c) depicts that the optical band gap is reduced to 3.49 eV as compared to that of reported ~3.9 eV for pure LN crystals.[57] The transparency with sharp absorption at 482 nm of grown crystal is much higher as compared to the earlier reported LN crystal[58] with much lower iron concentration (~0.028 mol%). Therefore, the Fe : LN crystal grown in the present study seems to be very good for the optical information processing[59] and holographic data storage applications.

Conclusions

An iron doped bulk single crystal of congruent Fe : LN has been successfully grown using low thermal gradient (LTG) two zone furnace by employing an indigenously developed crystal puller. The HRXRD revealed that the grown crystal has good crystalline perfection and does not contain macroscopic defects like grain boundaries and the dopants have occupied the vacant Li^+ sites. The obtained crystalline perfection also indicates the proper distribution of Fe in the crystalline lattice. The EPR analysis confirmed the proper axial incorporation of dopants at lithium sites. Prism coupler studies depicted the slight increment in refractive indices of LN with iron doping for ordinary and extraordinary rays with a refractive index change (Δn) of 0.0833. The UV-VIS-NIR studies revealed that the crystals are highly transparent for the wavelength range from 375 to 1100 nm and shows the lowering of band gap due to Fe-doping. The present studies reveal that the grown crystal with two zone LTG furnace has very good device properties which are needed for holographic data storage applications.

Acknowledgements

This work has been carried out under the Council of Scientific and Industrial Research (CSIR) project # OLP-070332. The authors are grateful to Prof. R. C. Budhani, Director, National Physical Laboratory, for his continuous encouragement for crystal growth activity at NPL. They sincerely thank Dr Chenna Dhanvantri, CEERI Pilani, for prism coupler measurements and Dr D. Haranath, NPL, New Delhi for fruitful discussions. SKK acknowledges the CSIR for providing Senior Research Fellowship (SRF).

Notes and references

1 Mark Haw, *Nature*, 2003, **422**, 556.
2 G. Assanto and I. Torelli, *Opt. Commun.*, 1995, **119**, 143.
3 H. Kang, C. X. Yang, G. G. Mu and Z. K. Wu, *Opt. Lett.*, 1990, **15**, 637.
4 J. F. Heanue, M. C. Bashaw and L. Hesselink, *Science*, 1994, **265**, 749.
5 H. Malcolm Dunn and Majid Ebrahimzadeh, *Science*, 1999, **286**, 1513.
6 K. Buse, A. Adibi and D. Psaltis, *Nature*, 1998, **393**, 665.
7 K. Peithmann, K. Buse and E. Kratzig, *Appl. Phys. B: Lasers Opt.*, 2002, **74**, 549.
8 K. Peithmann, A. Wiebrock and K. Buse, *Appl. Phys. B: Lasers Opt.*, 1999, **68**, 777.
9 M. Bayssie, D. Brownridge, N. Kukhtarev, T. Kukhtarev and J. C. Wang, *Nucl. Instrum. Methods Phys. Res., Sect. B*, 2005, **241**, 913.
10 H. Donnerberg, S. M. Tomlinson, C. R. A. Catlow and O. F. Schirmer, *Phys. Rev. B: Condens. Matter*, 1991, **44**, 4877.
11 Haixuan Xu, Donghwa Lee, Susan B. Sinnott, Venkatraman Gopalan, Volkmar Dierolf and Simon R. Phillpot, *Phys. Rev. B: Condens. Matter Mater. Phys.*, 2009, **80**, 144104.
12 G. Bhagavannarayana, P. Rajesh and P. Ramasamy, *J. Appl. Crystallogr.*, 2010, **43**, 1372.
13 G. Bhagavannarayana, R. V. Ananthamurthy, G. C. Budakoti, B. Kumar and K. S. Bartwal, *J. Appl. Crystallogr.*, 2005, **38**, 768.
14 P. C. Tsai, M. L. Sun, C. T. Chia, H. F. Lu, S. H. Lin, M. L. Hu and J. F. Lee, *Appl. Phys. Lett.*, 2008, **92**, 161902.
15 Dongfeng Xue and Xiangke He, *Phys. Rev. B: Condens. Matter Mater. Phys.*, 2006, **73**, 064113.
16 G. Bhagavannarayana, S. Parthiban and S. P. Meenakshisundarm, *J. Appl. Crystallogr.*, 2006, **39**, 784.
17 G. Bhagavannarayana and S. K. Kushwaha, *J. Appl. Crystallogr.*, 2010, **43**, 154.
18 G. Bhagavannarayana, G. C. Budakoti, K. K. Maurya and B. Kumar, *J. Cryst. Growth*, 2005, **282**, 394.
19 G. Bhagavannarayana, S. Parthiban and Subbiah Meenakshisundaram, *Cryst. Growth Des.*, 2008, **8**, 446.
20 Wenbo Yan, Yongfa Kong, Lihong Shi, Xiang Xie, Xiaochun Li, Jingjun Xu, Cibo Lou, Hongde Liu, Wanlin Zhang and Guangyin Zhang, *Phys. Status Solidi A*, 2004, **201**, 2013.
21 C. A. Wallace, *J. Appl. Crystallogr.*, 1970, **3**, 546.
22 N. V. Sidorov, M. N. Palatnikov, V. T. Gabrielyan, P. G. Chufyrev and V. T. Kalinnikov, *Inorg. Mater.*, 2007, **43**, 60.
23 K. Sugh, H. Iwasaki, S. Miyazawa and N. Nuzeki, *J. Cryst. Growth*, 1973, **18**, 159.
24 Z. I. Ivanova, A. I. Kovrigin, G. V. Luchinskii, N. Leonid Rashkovich, N. M. Rubinina and S. I. Kholodnykh, *Sov. J. Quantum Electron.*, 1980, **10**, 577.
25 B. J. Wicks and M. H. Lewis, *Phys. Status Solidi B*, 1968, **26**, 571.
26 P. Kumar, S. Moorthy Babu, I. Bhaumik, S. Ganesamoorthy, A. K. Karnal, A. K. Pandey and R. Raman, *Opt. Mater.*, 2010, **32**, 1364.
27 M. Kösters, B. Sturman, P. Werheit, D. Haertle and K. Buse, *Nat. Photonics*, 2009, **3**, 510.
28 A. M. Glass, D. Von der Linde and T. J. Negran, *Appl. Phys. Lett.*, 1974, **25**, 233.
29 K. K. Wong, *Properties of Lithium Niobate*, INSPEC, London, 2002, p. 123.
30 Xu Zhang and Dongfeng Xue, *J. Mater. Sci.: Mater. Electron.*, 1997, **8**, 133.
31 S. C. Abrahams, H. J. Levinstein and J. M. Reddy, *J. Phys. Chem. Solids*, 1966, **27**, 1019.
32 R. V. Ananthamurthy, K. S. Bartwal and Krishan Lal, *Mater. Sci. Eng., B*, 1993, **18**, L4.
33 G. Bhagavannarayana, S. K. Kushwaha, Mohd Shakir and K. K. Maurya, *J. Appl. Crystallogr.*, 2010, **44**, 122.
34 D. Cochet-Muchy, *J. Phys. IV*, 1994, **4**, C2-33.
35 S. H. Lee, Y. J. Kim, S. H. Cho and E. P. Yoon, *J. Cryst. Growth*, 1992, **125**, 175.
36 K. Lal and G. Bhagavannarayana, *J. Appl. Crystallogr.*, 1989, **22**, 209.
37 G. Bhagavannarayana, PhD thesis, University of Delhi, India, 1994.
38 A. Choubey, G. Bhagavannarayana, Yu. V. Shubin, B. R. Chakraborty and Krishan Lal, *Z. Kristallogr.*, 2002, **217**, 515.
39 S. K. Kushwaha, Mohd Shakir, K. K. Maurya, A. L. Shah, M. A. Wahab and G. Bhagavannarayana, *J. Appl. Phys.*, 2010, **108**, 033506.
40 K. Senthilkumar, S. Moorthy Babu and G. Bhagavannarayana, *J. Appl. Crystallogr.*, 2011, **44**, 313.
41 B. W. Batterman and H. Cole, *Rev. Mod. Phys.*, 1964, **36**, 681.
42 K. Lal, R. Ramanan and G. Bhagavannarayana, *J. Appl. Crystallogr.*, 2000, **33**, 2.
43 G. Bhagavannarayana, A. Chaubey, Y. Yu. Shubin and K. Lal, *J. Appl. Crystallogr.*, 2005, **38**, 448.
44 D. Staebler and W. Phillips, *Appl. Phys. Lett.*, 1974, **24**, 268.
45 M. Lee, S. Takekawa, Y. Furukawa, K. Y. Kitamura and H. Hatano, *Phys. Rev. Lett.*, 2000, **84**, 875.
46 Myekyu Lee, In Gyoo Kim, Shunji Takekawa, Yasunori Furukawa, Yoshishige Uchida, Kenji Kitamura and Hideki Hatano, *J. Appl. Phys.*, 2001, **89**, 5311.
47 J. B. Herrington, B. Dischler and J. Schneider, *Solid State Commun.*, 1972, **10**, 509.
48 R. Ulrich and R. Torge, *Appl. Opt.*, 1973, **12**, 2901.
49 Mingfu Zhang, Hengzhi Chen, Bin Yang and Wenwu Cao, *Appl. Phys. A: Mater. Sci. Process.*, 2009, **97**, 741.
50 Hidetoshi Onodera, Ikuo Awal and Jun-ichi Ikenoue, *Appl. Opt.*, 1983, **22**, 1194.
51 J. Imbrock, C. Baumer, H. Hesse, D. Kip and E. Kratzig, *Appl. Phys. B: Lasers Opt.*, 2004, **78**, 615.
52 D. Li, G. Ma, J. Ge, S. Hu and N. Dai, *Appl. Phys. B: Lasers Opt.*, 2008, **94**, 623.
53 P. Sen, P. K. Sen, R. Bhatt, S. Kar, V. Shukla and K. S. Bartwal, *Solid State Commun.*, 2004, **129**, 747.
54 O. F. Scirmer, O. Theimann and M. Wohlecke, *J. Phys. Chem. Solids*, 1991, **52**, 185.
55 M. Pape, H. J. Reyher and O. F. Schirmer, *J. Phys.: Condens. Matter*, 2005, **17**, 6835.
56 B. Andreas, K. Peithmann, K. Buse and K. Maier, *Appl. Phys. Lett.*, 2004, **81**, 3813.
57 L. Arizmendi, *Phys. Status Solidi A*, 2004, **201**, 253.
58 S. Kar, K. S. Sunil Verma and K. S. Bartwal, *Cryst. Growth Des.*, 2008, **8**, 4424.
59 Shiuan Huei Lin, Mei Li Hsieh, Ken Yuh Hsu, Tai Chiung Hsieh, Sheuan-Perng Lin, Tung-Sheng Yeh, Long-Jang Hu, Chin-Hwa Lin and Hong Chang, *J. Opt. Soc. Am. B*, 1999, **16**, 1112.

